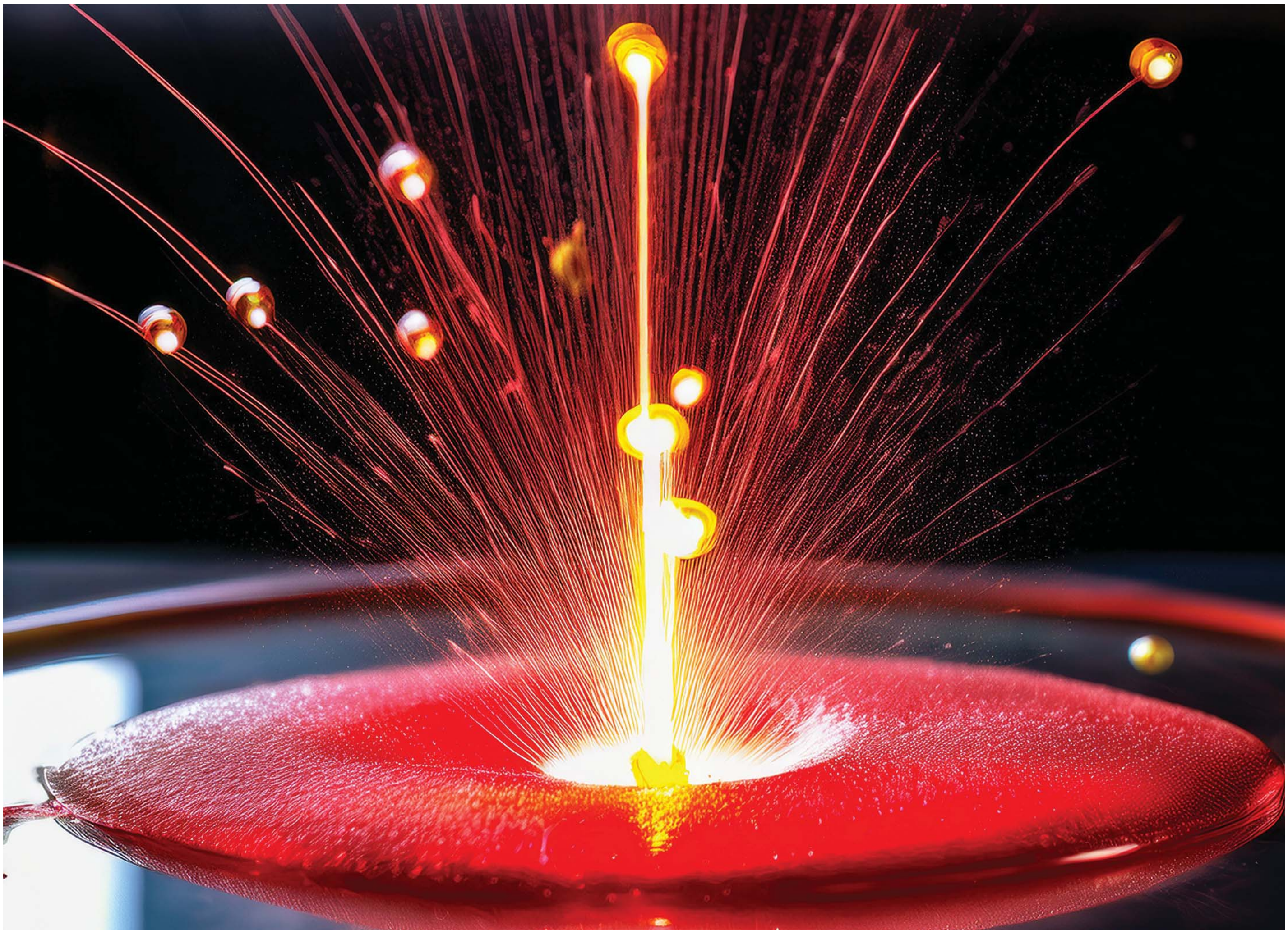

Showcasing research from MARTE Research Group (Unizar, Spain) and the Inorganic Analysis team (LGC National Measurement Laboratory, UK).

A novel particle mass calibration strategy for the quantification of AuNPs in single cancer cells *via* laser ablation ICP-mass spectrometry. A case study

This work proposes a particle mass calibration strategy that is independent of both the properties and thickness of the gelatin films used for calibration. This strategy relies on the individual ablation of nanoparticles (NPs) of well-characterized size that are embedded in the films, so that their mass can be directly used for calibration without the need to calculate their exact concentration within the gelatin. As a case study, quantitative analysis of HeLa cancer cells exposed to AuNPs is demonstrated.

Image reproduced by permission of Martín Resano from *J. Anal. At. Spectrom.*, 2025, **40**, 2673.

Image produced using Adobe Photoshop 2025 with its AI integrated tool, Adobe Firefly.

As featured in:

See Antonio Bazo *et al.*,
J. Anal. At. Spectrom.,
2025, **40**, 2673.

ROYAL SOCIETY OF CHEMISTRY

rsc.li/jaas

Registered charity number: 207890

JAAS

ROYAL SOCIETY OF CHEMISTRY

PAPER

View Article Online
View Journal | View Issue

Cite this: *J. Anal. At. Spectrom.*, 2025, **40**, 2673

A novel particle mass calibration strategy for the quantification of AuNPs in single cancer cells *via* laser ablation ICP-mass spectrometry. A case study

Antonio Bazo, *[a] Eduardo Bolea-Fernandez, [a] Kharmen Billimoria, [b] Ana Rua-Ibarz,[a] Maite Aramendía, [a] Paula Menero-Valdés, [b] Jack Morley,[b] Sara Neves,[b] Armando Sánchez-Cachero, [b] Heidi Goenaga-Infante [b] and Martín Resano [a]

Laser ablation ICP-mass spectrometry (LA-ICP-MS) has developed as a powerful tool for elemental quantitative analysis of individual cells, assuring that the content of each cell is analyzed individually. However, this technique is still limited by the difficulties associated with calibration using solid standards. This work proposes a particle mass calibration strategy that is independent of both the properties and thickness of the gelatin films used for calibration, overcoming a significant drawback of previously established methods. The fundamental principle of this strategy relies on the individual ablation of nanoparticles (NPs) of well-characterized size that are embedded in the films, so that their mass can be directly used for calibration without the need to calculate their exact concentration within the gelatin. The performance of the newly developed method was compared to that of the previously reported approaches (ionic and particle number calibration) in terms of linearity and homogeneity between different films prepared from the same gelatin solution. As a case study, the three calibration strategies were used for the quantitative analysis of HeLa cancer cells exposed to AuNPs. In parallel, in-suspension single-cell (SC) ICP-MS Au data were obtained and used as reference for comparison with the three LA-SC-ICP-MS strategies. The results obtained with the novel particle mass approach demonstrated better accuracy and repeatability over three different working sessions, addressing key limitations and providing a robust and reliable method for quantitative LA-SC-ICP-MS analysis. The particle mass method holds promise for quantitative LA-ICP-MS analysis of samples beyond NP-exposed cells, such as biological tissues.

Received 30th June 2025
Accepted 11th August 2025

DOI: 10.1039/d5ja00253b

rsc.li/jaas

[a] *University of Zaragoza, Department of Analytical Chemistry, Aragon Institute of Engineering Research (I3A), Zaragoza, Spain, 50009. E-mail: abazo13@gmail.com*
[b] *National Measurement Laboratory, LGC Limited, Queens Road, Teddington, London, UK*

Antonio Bazo obtained his degree in Chemistry at the University of Zaragoza (Spain) in 2020. After obtaining a Master degree in Nanostructured Materials for Nanotechnology Applications from the same university, he is currently a PhD student at the Department of Analytical Chemistry in the Rapid Analysis Methods with Spectroscopic Techniques – MARTE – research group, belonging to the Aragon Institute for Engineering Reseach (i3a). His research focuses on fundamentals and applications of single-particle/cell ICP-mass spectrometry (SP/SC-ICP-MS), submitting nine different articles to high-impact scientific journals and attending five conferences during his PhD. The public defense of his PhD thesis, titled "Improving Quantification in Single-Event Inductively Coupled Plasma Mass Spectrometry", is scheduled for late 2025.

1. Introduction

Breakthroughs in nanotechnology have enabled the design of new drug delivery vectors significantly superior to prior drugs in terms of both pharmacokinetics and pharmacodynamics.[1–3] Among these new nanomaterials, noble metal nanoparticles, including Ag, Au, Pd, and Pt nanoparticles (NPs), are of special interest in cancer research. These NPs offer high biocompatibility, controllable shape and size, and surface properties that allow for suitable modification to bind drugs and ligands.[4,5] Above all metal-based NPs, AuNPs have proven their applicability as drug nanocarriers, contrast agents, radiosensitizers, and thermal therapy agents, making them particularly relevant.[6]

Therefore, analytical methods that allow for quantification of the uptake of AuNPs within tumor cells are in high demand for the development of cancer therapies. In this context, conventional bulk analyses provide valuable information on the average content of Au per cell in a cell suspension.[7] However, meaningful information is lost with these approaches, given that the natural heterogeneity and time dynamics within the cell population are not considered.[8–10] Applying single-cell (SC) methodologies is thus preferred, so cells can be monitored individually, and the AuNP uptake distribution within the cell population can be obtained, rather than only its average concentration. This allows for the evaluation of the heterogeneity of the sample and the identification of cells with anomalous analyte contents. Inductively coupled plasma-mass spectrometry (ICP-MS) is a reference technique that, despite being originally designed for the analysis of homogeneous aqueous solutions, can be operated in single-event mode for the monitoring of discrete entities, such as nano/microparticles, cells, and even microplastics, present in heterogeneous aqueous suspensions.[11–14] This advancement is a result of instrumental and methodological improvements that allow for the monitoring of the ultra-fast transient signals (~500 μs) that characterize such entities.[12,15]

Whilst being able to provide such valuable information, SC-ICP-MS still faces significant difficulties with the transport of cell suspensions into the ICP, given both the fragility and relatively large size of the cells (up to 100 μm).[10] Therefore, sample introduction setups should maximize both the cell integrity during the introduction and the transport efficiency (TE) (*i.e.*, the ratio between the number of cells detected compared to those introduced into the system). For this purpose, different high-efficiency nebulizers and spray chambers have been specifically developed for SC analyses, but they still cannot ensure either cell integrity or complete transport.[16,17] These phenomena may jeopardize the validity of the results, particularly for large and fragile cells, for two different reasons. First, if cell lysis occurs during sample introduction, the internalized NPs will be released, potentially leading to incorrectly attributing these NP events to cell events. Second, if the TE is not the same for the entire range of cell sizes introduced, the registered mass histogram will also be biased in favor of the better-transported cells. In addition to these issues, there is also the possibility of monitoring double events (*i.e.*, the simultaneous detection of several cells), leading to abnormally intense signals.[12] The occurrence of double events can be minimized by using a sufficiently diluted suspension, but even then, some cells tend to agglomerate and, therefore, increase the chance of being simultaneously detected and cause blockages in the sample line. This is especially problematic when the mass distribution does not follow any clear mathematical model, as there will be no valid statistical criteria for outlier rejection.

To circumvent the difficulties associated with the introduction of cells in aqueous suspensions, laser ablation (LA) can be coupled to ICP-MS instrumentation. This setup has been widely used for the direct analysis of solid samples, as it combines the spatial resolution of the laser system with the high selectivity and sensitivity of the ICP-MS instrument. Therefore, LA-ICP-MS can be used for the analysis of individual cells, selecting them one by one for their subsequent ablation, so that all the ejected material can then be transported into the ICP, ensuring that each transient signal corresponds to an individual cell. Nevertheless, the preparation of suitable calibration standards for quantitative LA-SC-ICP-MS, and LA-ICP-MS in general, remains a challenge when compared to the in-suspension counterpart, given the limited availability of commercial solid calibration standards.[18–20] In response, several strategies have been proposed in the literature for the preparation of in-house solid calibration standards, including gelatin droplets, films and cryosections, spiked filters, and agarose films, among others.[20–26]

Gelatin calibration standards are of particular interest due to the relative ease of preparation and capability for matrix-matching for both tissue and cell samples.[24,27] This strategy relies on spiking the gelatin matrix with standard solutions containing either ionic standards or monodisperse NPs with well-known concentrations, so that the concentration of the analyte in the final film of dried gelatin can be calculated. Such calculations require both the density and thickness of the films prepared in this way to be homogeneous and well-characterized to avoid biased results. Additionally, manual approaches for the preparation of gelatin calibration standards, such as cryosectioning, often require skilled users and still suffer from poor reproducibility. To overcome these issues, methods that incorporate automated instrumentation, such as bioprinters, have demonstrated better performance, not only in terms of preparation time but also regarding homogeneity, as they deposit a consistent amount of gelatine for each film without applying any external force that might damage the standard.[26]

2. Experimental

2.1 Instrumentation

All MS data were acquired using an icpTOF 2R time-of-flight (ToF) ICP-mass spectrometer (TOFWERK, Thun, Switzerland) operated in transient mode. This ICP-ToF-MS device was coupled to an ImageBIO 266 nm LA system equipped with a TwoVol3 ablation chamber and a dual concentric injector interface (ESI, Bozeman, EEUU). Analysis of suspended cells was carried out using a Single Cell Introduction Kit (ESI) consisting of a Cytoneb 50 nebulizer, a CytoSpray chamber, and a one-piece torch. Instrument settings and data acquisition parameters used for the analysis of gelatins and cells, as well as the LA operating conditions, are summarized in Tables S1 and S2 of the SI, respectively.

2.2 Gelatin standards preparation and analysis

For the ionic gelatin-based calibration, 10% (w/w) porcine gelatin (300 bloom strength) solutions spiked with five different concentrations of an ionic Au reference solution (1000 mg kg^{-1}, ROMIL, Cambridge, UK) were prepared in ultrapure 18.2 MΩ cm water (ELGA water, High Wycombe, UK) and heated to 60 °C until fully dissolved. Gelatin solutions were frozen and cryo-sectioned (20 μm) with a cryotome (Leica Biosystems, CM1850, Nussloch, Germany). Sections were placed onto a microscope slide and air dried for 24 hours at ambient conditions, obtaining a final thickness of 2 μm for the dried films, as characterized by multiphoton fluorescence microscopy in a precedent article in which the RSD is estimated to be 12%.[26] Therefore, for a spot size of 20 μm, the ablated volume per shot is 628 μm^3.

For both the particle number and particle mass calibration strategies, 1% (w/w) gelatin solutions were prepared in ultrapure 18.2 MΩ cm water and spiked with AuNPs. In the case of the particle number approach, different concentrations of the 30 nm AuNP (Quality Control Material LGCQC5050, 32.7 ± 2.0 nm (LGC, London, UK)) standard suspension used for cell exposure were also used to achieve average concentrations of 0, 1, 5, 10 and 25 NPs per ablated spot. For the particle mass strategy, gelatin films with an average number of NPs per ablation area of 0.15 were prepared using 50 nm (49.9 ± 1.9 nm), 55 nm (54.9 ± 2.1 nm) UltraUniform™, and 100 nm (98 ± 7 nm) BioPure™ AuNPs (Nanocomposix Europe, Prague, Czech Republic), and 60 nm (HiQ-Nano, Arnesano, Italy; 60 ± 3.5 nm) AuNP standards. Average sizes obtained from the certificate of analysis of the manufacturer. Solutions were heated to 60 °C and mixed thoroughly. A Bio X6 bioprinter (CELLINK, Göteborg, Sweden) was then used for printing gelatin droplets onto a microscope slide. The gelatin solutions with suspended AuNPs were loaded into the bioprinter pneumatic head, and droplets were printed using a 5 kPa extrusion force for 0.03 s. Using such conditions, 1 mg droplets were obtained. Slides were air dried for 24 h under ambient conditions, again obtaining a final dry thickness of 2 μm (RSD of 16%), as determined *via* multiphoton fluorescence microscopy. Under these conditions, the ablated volume is again of 628 μm^3.

2.3 HeLa cells sample preparation and isolation

HeLa cells (American Type Culture Collection, CCL-2, Manassas, EEUU) were seeded at a density of 3×10^6 cells per flask in T75 flasks and were allowed to adhere for 24 hours. After this time, the culture medium was replaced with AuNPs-containing fresh medium (1 mg per mL AuNPs) without fetal bovine serum (see SI), and the cells were incubated for another 24 hours. Following the incubation with AuNPs, cells were rinsed with phosphate-buffered saline (PBS; Gibco, Jenks, EEUU) before adding Accutase (StemPro Accutase Cell Dissociation Reagent; Gibco), and incubated at 37 °C for 5 minutes until they were detached. The cell suspension was centrifuged at 1200 rpm for 5 minutes before resuspension in PBS. After this protocol, the cells were fixed with 4% PFA and kept in the fridge. Cell density and viability were assessed using Vi-CELL™ XR Cell Viability Analyzer (Beckman Coulter Inc., Brea, EEUU). Both single-cell sorting and isolation were performed using the CellenONE® X1 (SCIENION, Berlin, Germany), which utilizes an image-based detection system combined with an acoustic dispensing technology for the sorting of single cells. For further information on cell preparation, sorting, and isolation, see the SI.

2.4 Data processing

Every dataset from the ionic and particle number calibration strategies was directly processed to calculate the average intensity and standard deviation with the OriginPro software (version 2021b, 9.85), which was also used for charts, fittings, and interpolations. Raw data from the particle mass calibrations were processed with an in-house developed script, discussed elsewhere,[28] to integrate all the intensity points corresponding to the same NP and subsequently subtract the contribution from the gelatin (average intensity of the regions of the droplet not containing NPs). Then, the signal intensities of the NPs were fitted to Gaussian distributions so that the central value was selected as the analytical signal. Finally, cell and in-suspension NP datasets were processed using the Hyper Dimensional Image Processing (HDIP v1.8.4, Teledyne Photon Machines, Belgrade, EEUU) software, and the signals were adjusted to LogNormal and Gaussian distributions, respectively, to obtain the mode of the fitted functions.

3. Results and discussion

As previously mentioned, two different approaches for gelatin-based calibration have been proposed in the literature so far, depending on the nature of the analyte standards embedded in the films: (i) ionic calibration, and (ii) particle number calibration. The former method is based on introducing a certain volume (V_{ion}, in cm^3) of an ionic standard of well-known concentration (C_{ion}, in fg cm^{-3}) during the preparation of the gelatin, whereas the second one incorporates a certain volume (V_{std}, in cm^3) of an NP standard suspension of well-known particle number concentration (PNC, in cm^{-3}) and well-characterized NP mass (m_{NP}, in fg). Then, for a given spot size (d, in μm) and mass of gelatin powder (m_{gelatin}, in g), provided that both the thickness (h, in μm) and density (ρ, in g cm^{-3}) of the final film are well characterized, the analyte mass ablated per shot (m, in fg) can be calculated according to eqn (1) and (2).

$$m_{\text{ionic}} = \frac{\pi\, d^2\, h\, \rho\, V_{\text{std}}\, C_{\text{ion}}}{4\, m_{\text{gelatin}}} \times 10^{-12} \tag{1}$$

$$m_{\text{particle number}} = \frac{\pi\, d^2\, h\, \rho\, V_{\text{std}}\, P\,N\,C\, m_{\text{NP}}}{4\, m_{\text{gelatin}}} \times 10^{-12} \tag{2}$$

Therefore, by modifying either the concentration of the standards or the volume introduced during the preparation of the gelatin (or, alternatively, the ablation area),[29] a different analyte mass will be ablated per shot, allowing for a calibration curve to be constructed by monitoring the average intensity from the ablated area (approx. 20–50 scan lines). Both methods stand out for their simplicity in terms of data processing; however, eqn (1) and (2) also evidence the main weaknesses of these calibration strategies. First, they require the complete ablation of the gelatin to calculate the amount of material ejected per shot. Second, they are affected by multiple sources of error, including those related to instrumental parameters like the spot size, uncertainties inherent to the characterization of the gelatin, and random errors occurring during the preparation and weighing of the standards. Finally, errors in the measurement or assumptions in the determination of the thickness of the film would lead to biased results.

This work proposes and evaluates a new approach based on particle mass to overcome the intrinsic difficulties of controlling the properties and thickness of the film. This method, independent of these potential sources of variation and uncertainty, relies on preparing the different gelatin films with NP

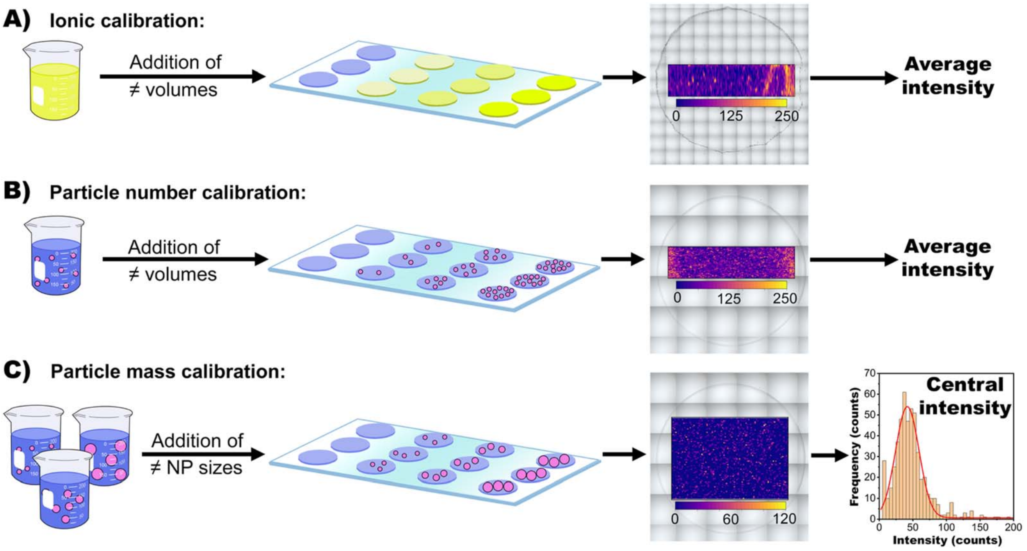

Fig. 1 Schematic representation of the differences in preparation, analysis, and data processing for the ionic (A), particle number (B), and particle mass (C) gelatin-based calibration approaches.

standards of different sizes at a very low concentration level (0.15 NPs per ablation spot) to limit the possibility of having multiple NPs per spot, thus enabling their individual ablation and transport of their analyte content to the ICP. Calibration curves are simply constructed by plotting the average intensity (evaluated as the central value of the Gaussian function adjusted to the intensity histogram) of each NP standard *versus* its corresponding mass (m_{NP}, in fg), calculated from its reference diameter (d_{NP}, in nm), characterized by transmission electron microscopy (TEM), and its density (ρ_{NP}, in g cm^{-3}), according to eqn (3). Therefore, the only source of error, as for any NP-based calibration, is the characterization of the particle diameters, which given the high precision of the TEM measurements, should have minimal impact on the results. As compared to the ionic and particle number calibration approaches, the particle mass requires more scan lines (approx. 50–100) to register sufficient events for obtaining a clear distribution, provided that the gelatin films are very diluted in NPs. This new approach, along with the established ones, is schematized in Fig. 1.

$$m_{\text{particle mass}} = \frac{\pi\, d_{\mathrm{NP}}{}^{3}\, \rho_{\mathrm{NP}}}{6} \times 10^{-6} \tag{3}$$

3.1 Method development and optimization

As discussed earlier, a prerequisite for the successful application of the traditional gelatin-based calibration approaches is to ensure that the LA operating conditions allow for full ablation of the entire section of the film being focused. Parameters such as fluence and scan speed impact the ablation performance and require optimization. For example, laser fluence can be increased to ablate the entire thickness of the material, but this increase has limitations. When the energy exceeds a certain threshold, the area adjacent to the focused spot is also affected by the beam, resulting in abnormally high-intensity readings (caused by the indirect ablation of the surroundings) and changes in the structure and dimensions of the film (as the nearby gelatin melts down and/or small chunks are removed and ejected to different positions). Therefore, two instrumental parameters needed to be optimized. First, the laser fluence was fixed to 4 J cm^{-2}, as it was the maximum energy that did not induce the formation of thermal effects in the vicinity of the shot spots when performing a single firing. Then, the scan speed can be tuned by either modifying the repetition rate (*i.e.*, the number of pulses emitted per second) or the spot size, as the former parameter is defined as the product of the latter two (full ablation per shot is accomplished). In this work, the spot size was fixed at 20 µm for all the calibration approaches, and the repetition rate was optimized from the values eligible in the software (5, 10, 20, 50, and 100 Hz), leading to scan speeds of 100, 200, 400, 1000, and 2000 µm s^{-1}, respectively. Fig. 2 shows the optimization of this parameter for both the ionic (Fig. 2A) and the particle number (Fig. 2B) calibration approaches. Results suggest that, regardless of the nature of the Au standard of choice, increasing the repetition rate also increases the average intensity monitored, as the amount of gelatin ablated increases, until a sort of plateau is achieved for 20 Hz. After this point, the total ablation of the gelatin is achieved, as shown in the inset pictures of Fig. 2, so further increases in the repetition rate increase the impact of thermal effects around the shot area and ablation craters larger than the desired resolution, leading to higher imprecision and only a slight enhancement of the intensity recorded. Therefore, 20 Hz (scan speed of 400 µm s^{-1}) was the selected repetition rate for the application of the ionic and particle number calibration approaches.

This paradigm significantly changes for the proposed particle mass calibration since it does not require the full ablation of the films, but the individual monitoring of the embedded NPs, which allows for the use of low repetition rates. In this context, increasing the repetition rate, and thus the scan speed, not only interferes with the homogeneous ablation of the

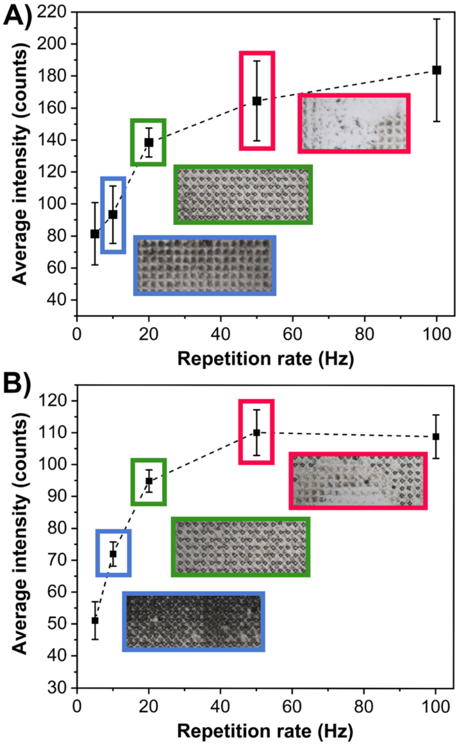

Fig. 2 Effect of the repetition rate on both the structure and intensity monitored for gelatin standards containing 9.85 fg of ionic Au standard per spot (A) and 3.6 fg of 32.7 nm AuNPs per spot (B). Error bars represent the standard deviation of the different films analyzed ($n = 3$). Inset pictures show the microscopic images of the sampled area after ablation.

gelatin but can also spread the signal corresponding to a single NP over multiple pixels. As shown in Fig. 3A, this effect was observed when the signal duration exceeded the time available for the instrument to collect the signal for each pixel (inverse of the repetition rate, referred to as time period), which resulted in aliasing. Therefore, if pixel resolution is lost, raw intensity values cannot be directly plotted in a histogram, since low-intensity outliers (corresponding to readings at the end of the NP ion cloud that are misattributed to adjacent pixels) appear with a frequency that grows as the repetition rate also increases. This phenomenon is evidenced in Fig. 3B, where the actual NP intensity distribution is only observed at a repetition rate of 5 Hz, while for the rest of the values, no distribution is observed or, in case it can be distinguished, it presents an abnormally low intensity as the ionic clouds are not being registered in their totality. Although a repetition rate of 5 Hz could be selected for the development of the method, it would also involve longer analysis times, thus limiting the applicability of this calibration method. To circumvent this issue, it is possible to further process the data in order to identify and add together all the values belonging to the same NP (time-resolved analysis), rather than constructing the histogram with every raw intensity reading. For this purpose, an in-house-developed script for conventional single-event ICP-MS, discussed elsewhere,[28] was adapted to identify the limits of the intensity events for their subsequent integration. With this strategy, it was possible to obtain clear distributions at every repetition rate, as represented in Fig. 3C. However, pseudo-double events (*i.e.*, integrating together intensity values corresponding to different NPs) appeared more frequently as the rate increased, given that the events broadened so much that they merged with the adjacent ones, leading to the registration of secondary distributions in the histograms. Mathematical deconvolutions can then be used to correct for these overlaps, but their performance is limited for smaller NPs, even if they are monodisperse. Additionally, the impact of the background on the integrated intensity increases with the number of pixels contributing to the signal, negatively affecting the precision. For all these reasons, 10 Hz was the selected repetition rate for this approach, using the time-resolved analysis script for data processing. Developing more advanced scripts for this application could significantly reduce the analysis time, but this is considered beyond the scope of the present, proof-of-concept work.

3.2 Application to the analysis of AuNP-doped HeLa cells: comparison with in-suspension SC-ICP-MS

To evaluate the performance of the different calibration approaches, three batches of gelatin standards were prepared on different days and analyzed along with the HeLa cells during separate working sessions. Additionally, three different films were evaluated for each of the five calibration points to assess the variability inherent to their preparation. Table 1 shows the linearity (evaluated as the R^2 of the linear regression) and average RSD per calibration point ($n = 3$) for each calibration strategy across all measurement sessions. All the calibration curves were constructed with a blank and four different points, covering a range from 0 to 10 fg per spot. The results indicate that the best linearity with the lowest variability is obtained for the particle mass calibration approach, as well-characterized NPs were used throughout the work, thus minimizing biases associated with the calculation of the mass per NP. The greater variability between the three sessions for the ionic and particle number calibration approaches can be attributed to the difficulties associated with the control of both the NP number concentration (for the particle number calibration) and the thickness of the gelatin, which are especially significant when using cryosections (for the ionic calibration), as films can be damaged during deposition onto the microscope slide.[26] These differences between systems for the preparation of gelatin films are also evidenced in the registered RSDs, as a lower variability between films prepared from the same gelatin solution is observed for those prepared by bioprinting compared to the cryotome. Again, the novel particle mass calibration provides the lowest RSD values, as it is unaffected by the bioprinter performance.

For the HeLa cells, approximately 200 cells were deposited onto a microscope slide every session for individual whole-cell ablation. Then, all the events were quantified using the three calibration approaches to obtain their Au mass per individual cell, from which the mass distribution of the cell population could be compared. This strategy is of particular interest, as it ensures that all the registered events correspond to individual

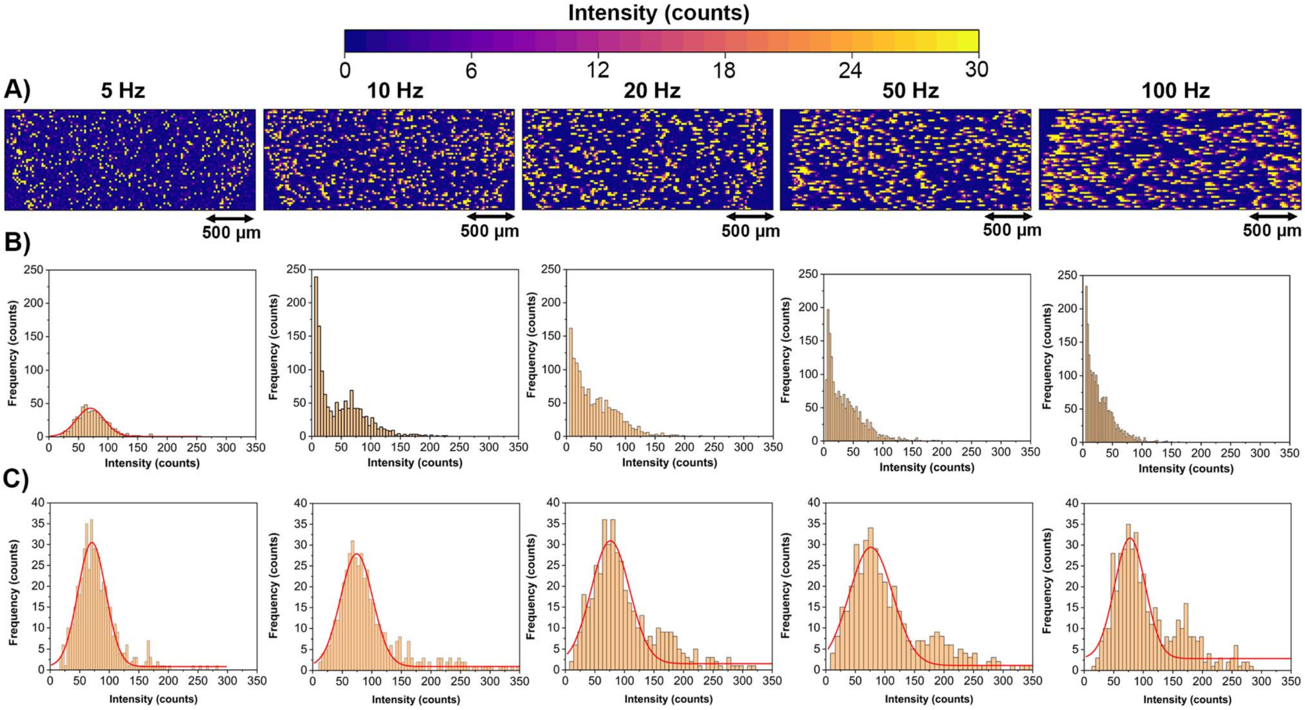

Fig. 3 Effect of the repetition rate on the Au elemental map images (A), raw intensity histogram (B), and time-resolved analysis intensity histograms (C) for gelatin standards containing 60 nm AuNPs.

cells, eliminating the impact of double events on mass distributions. In addition, by individually selecting the cells to be ablated, the total number of cells analyzed is known, making it easier to verify whether part of the population is below the limit of detection by simply comparing the number of events recorded with the number of shots performed, which always matched in this work for all the sessions (100% transport efficiency). Therefore, provided that the distributions registered are representative of the cell population, the function that best fits such a distribution can be identified. In this case, the LogNormal distribution was found to be the best fit for the cell population (Fig. 4A). This observation is in good agreement with previous works that studied the intake of NPs by cells, and the positive tail could be attributed to the phagocytosis of NP agglomerates formed out of the cell.[30]

To corroborate the LA-SC-ICP-MS results obtained using the different calibration strategies, in-suspension SC-ICP-MS was used as the reference method. For this purpose, the different AuNP standards were measured in single-event mode, so that a calibration curve was constructed with the central intensities

Table 1 Comparison of the linearity (R^2), and average RSD per calibration point monitored for the different calibration approaches during three working sessions

	R^2			
Calibration approach	Session 1	Session 2	Session 3	Average[a]
Ionic	0.9997	0.9978	0.9992	0.9989 ± 0.0010
Particle number	0.9935	0.9985	0.9989	0.9970 ± 0.0030
Particle mass	0.9999	0.9997	0.9997	0.9998 ± 0.0001
	Average RSD per calibration point (%)			
Calibration approach	Session 1[b]	Session 2[b]	Session 3[b]	Average[a]
Ionic	10.69 ± 2.68	6.51 ± 2.08	11.28 ± 3.78	9.49 ± 2.60
Particle number	6.20 ± 1.67	5.42 ± 2.83	8.27 ± 4.74	6.63 ± 1.48
Particle mass	2.26 ± 0.70	1.79 ± 0.77	3.22 ± 1.51	2.42 ± 0.73

[a] Imprecision expressed as standard deviation between sessions. [b] Imprecision represents the standard deviation of the five different calibration points.

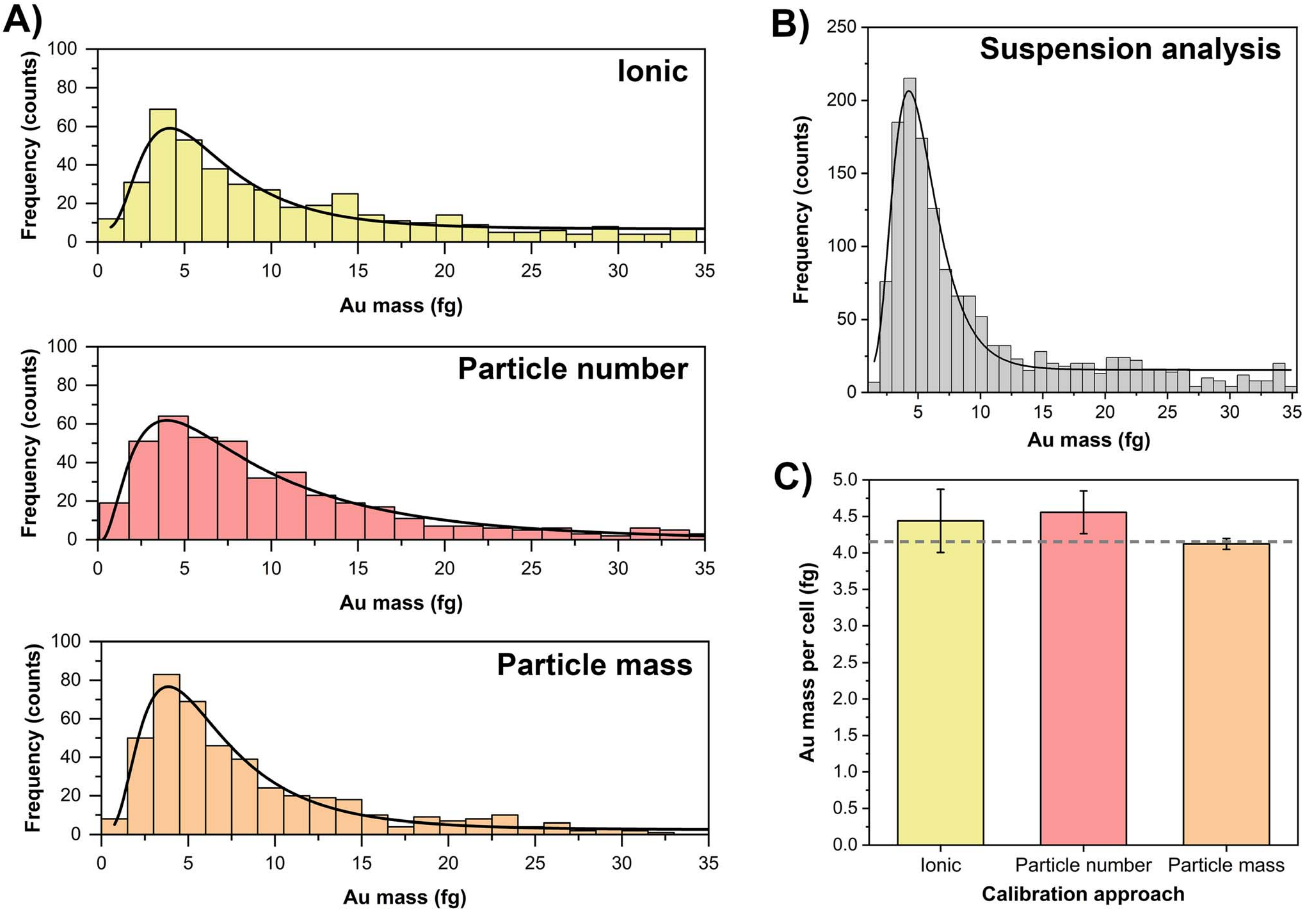

Fig. 4 Sum mass distributions obtained for the LA analysis of HeLa cells exposed to AuNPs with the three different calibration approaches (A), and in-suspension analysis (B), along with the comparison of the mode of the adjusted LogNormal functions registered for each strategy during each session with their standard deviation (C). The gray line in (C) represents the reference value obtained from (B).

of their adjusted normal distributions (*i.e.*, external calibration).[31] Then, the diluted cell sample suspension (5×10^4 cells per mL) was introduced into the system to keep the statistical probability of double events below 0.1%, and the events were interpolated in the curve, obtaining the distribution shown in Fig. 4B. Despite statistically limiting the occurrence of double events, the solution-based method does not provide as much control as the LA one, and the distribution can still be affected by double events or cell aggregates, which makes the mathematical comparison of the results more difficult.

Therefore, the mathematical parameters typically used to compare results in single-event ICP-MS, such as the mean or the median, are not eligible in this case, as abnormally high values are obtained for the in-suspension measurements. Moreover, using the mode of the individual measurements is not recommended, given the relatively low number of cells evaluated with the LA analysis (200 cells). Thus, the mode of the adjusted LogNormal distribution (*i.e.*, the mass value at which the first derivative of the fitted function is zero) was found to be a more adequate parameter for the comparison of both single-cell approaches, given that this parameter is not affected by double events (*i.e.*, the function is deconvoluted from the original distribution), and it is also more consistent than the mode of the single values themselves. Therefore, the results obtained with the different calibration approaches for LA-SC-ICP-MS and those of in-suspension SC-ICP-MS were compared by using the mode of the adjusted functions, leading to the results shown in Fig. 4C. As can be seen, the best accuracy and repeatability (represented by the lower error bar indicative of the standard deviation of the three working sessions) are achieved for the proposed particle mass method. However, no significant differences were observed for any of the calibration strategies at a 95% confidence level (reference suspension analysis: 4.19 fg; ionic calibration: 4.44 ± 1.08 fg; particle number calibration: 4.56 ± 0.73 fg; particle mass calibration: 4.12 ± 0.18 fg), which indicates that all three approaches can be used depending on the specific needs.

4. Conclusions

In this work, a novel particle mass-based approach for preparing gelatin calibration standards is proposed for LA-SC-ICP-MS analysis. The strategy is based on the individual monitoring of NPs of well-characterized mass in a gelatin matrix, so that a calibration curve can be constructed by analyzing films containing NPs of different sizes, covering a wide mass range. For this methodology, a very low concentration of NPs needs to be used for the preparation of gelatin standards (0.15 NPs per ablation spot to avoid the ablation of multiple NPs per individual laser shot), and the time-resolved analysis of the signals was performed to correct for the aliasing observed for repetition rates above 10 Hz. As compared to the ionic and particle number calibration strategies, the novel particle mass method exhibited better linearity and less variability between films prepared from the same gelatin solution. As a case study, the performance of this method was successfully evaluated for the analysis of HeLa cancer cells exposed to AuNPs, obtaining better accuracy and repeatability than the former calibration strategies over three different working sessions.

This novel calibration strategy provides a robust methodology for LA-SC-ICP-MS analysis. It guarantees that the results correspond exactly to each cell, and thus, the distributions obtained reflect the true heterogeneity of the cell population, circumventing the problems typically associated with the transport of large cells to the ICP in the case of solution-based SC-ICP-MS analysis.

Moreover, it is important to stress that while the method proposed was developed to monitor inorganic NPs in single cells, as a relevant and distinctive field of application for LA-ICP-MS, this strategy is neither limited to single-cell analysis nor to NPs characterization. It provides a calibration value per analyte mass that can be used for any quantitative LA-ICP-MS analysis, as long as well-characterized NPs containing the analyte of interest are available.

Author contributions

A. B.: conceptualization, methodology, validation, formal analysis, investigation, data curation, writing – original draft. E. B.-F. and A. R.-I.: conceptualization, writing – review and editing, visualization, supervision. K. B.: formal analysis, supervision, writing – review and editing. M. A.: visualization, supervision. P. M.-V. and A. S.-C.: formal analysis, investigation, writing – review and editing. J. M. and S. N.: resources. H. G.-I.: resources, writing – review and editing, project administration. M. R.: resources, supervision, writing – review and editing.

Conflicts of interest

The authors declare no competing financial interests.

Data availability

Data for this article are available at Zenodo at **https://zenodo.org/records/16358932**.

SI on the measurement conditions and cell preparation is available. See DOI: **https://doi.org/10.1039/d5ja00253b**.

Acknowledgements

The authors are grateful to the European Regional Development Fund ("ERDF A way of making Europe") for financial support through the Interreg POCTEFA Nanolyme EFA99/1, to project PID2021-122455NB-I00 (funded by MCIN/AEI/10.13039/501100011033 and by ERDF) and to the Aragon Government (Grupo E43_20R and PROY_E17_24). We also thank the I3A Impulso call, the Ibercaja Foundation, and the University of Zaragoza. A. B. acknowledges the Department of Science, University and Knowledge Society from DGA for his predoctoral grant (2021 call). E. B.-F. acknowledges financial support from the Ramón y Cajal programme (RYC2021-031093-I) funded by MCIN/AEI/10.13039/501100011033 and the European Union (NextGenerationEU/PRTR). A. R.-I. thanks the European Union's Horizon 2020 research and innovation program under the Marie-Sklodowska-Curie grant agreement no. 101034288. Authors also thank the UK Department for Science, Innovation and Technology for funding.

References

1 B. Kang, M. M. Afifi, L. A. Austin and M. A. El-Sayed, *ACS Nano*, 2013, **7**, 7420–7427.
2 R. M. Kannan, E. Nance, S. Kannan and D. A. Tomalia, *J. Intern. Med.*, 2014, **276**, 579–617.
3 L. Cohen, Y. D. Livney and Y. G. Assaraf, *Drug Resistance Updates*, 2021, **56**, 100762.
4 S. R. Oliveira, K. Tuttis, A. R. T. Machado, C. C. de Souza Rocha, L. M. G. Antunes and F. Barbosa, *Microchem. J.*, 2022, **177**, 107275.
5 R. Zhao, J. Xiang, B. Wang, L. Chen and S. Tan, *Bioinorg. Chem. Appl.*, 2022, **2022**, 2444516.
6 K. K. Jain, in *Drug Delivery Systems*, ed. K. K. Jain, Springer, New York, NY, 2020, pp. 1–54.
7 X. Wei, D.-H. Zheng, Y. Cai, R. Jiang, M.-L. Chen, T. Yang, Z.-R. Xu, Y.-L. Yu and J.-H. Wang, *Anal. Chem.*, 2018, **90**, 14543–14550.
8 H. Wang, B. Chen, M. He, X. Li, P. Chen and B. Hu, *Talanta*, 2019, **200**, 398–407.
9 Y. Cao, J. Feng, L. Tang, C. Yu, G. Mo and B. Deng, *Talanta*, 2020, **206**, 120174.
10 T. Liu, E. Bolea-Fernandez, C. Mangodt, O. De Wever and F. Vanhaecke, *Anal. Chim. Acta*, 2021, **1177**, 338797.
11 E. Bolea-Fernandez, A. Rua-Ibarz, M. Velimirovic, K. Tirez and F. Vanhaecke, *J. Anal. At. Spectrom.*, 2020, **35**, 455–460.
12 M. Resano, M. Aramendía, E. García-Ruiz, A. Bazo, E. Bolea-Fernandez and F. Vanhaecke, *Chem. Sci.*, 2022, **13**, 4436–4473.
13 P. Menero-Valdés, M. I. Chronakis, B. Fernández, C. D. Quarles Jr, H. González-Iglesias, B. Meermann and R. Pereiro, *Anal. Chem.*, 2023, **95**, 13322–13329.
14 T. Vonderach, A. Gundlach-Graham and D. Günther, *Anal. Bioanal. Chem.*, 2024, **416**, 2773–2781.
15 B. Meermann and V. Nischwitz, *J. Anal. At. Spectrom.*, 2018, **33**, 1432–1468.
16 C. Davison, D. Beste, M. Bailey and M. Felipe-Sotelo, *Anal. Bioanal. Chem.*, 2023, **415**, 6931–6950.
17 S. Theiner, K. Loehr, G. Koellensperger, L. Mueller and N. Jakubowski, *J. Anal. At. Spectrom.*, 2020, **35**, 1784–1813.

18 E. Hoffmann, C. Lüdke and H. Scholze, *Fresenius. J. Anal. Chem.*, 1997, **359**, 394–398.

19 J. Pisonero, B. Fernández and D. Günther, *J. Anal. At. Spectrom.*, 2009, **24**, 1145–1160.

20 N. Miliszkiewicz, S. Walas and A. Tobiasz, *J. Anal. At. Spectrom.*, 2015, **30**, 327–338.

21 H.-J. Stärk and R. Wennrich, *Anal. Bioanal. Chem.*, 2011, **399**, 2211–2217.

22 R. J. C. Brown, K. E. Jarvis, B. A. Disch and S. L. Goddard, *Int. J. Environ. Anal. Chem.*, 2013, **93**, 335–348.

23 D. J. Hare, J. Lear, D. Bishop, A. Beavis and P. A. Doble, *Anal. Methods*, 2013, **5**, 1915–1921.

24 M. Šala, V. S. Šelih and J. T. van Elteren, *Analyst*, 2017, **142**, 3356–3359.

25 K. Billimoria, D. N. Douglas, G. Huelga-Suarez, J. F. Collingwood and H. Goenaga-Infante, *J. Anal. At. Spectrom.*, 2021, **36**, 1047–1054.

26 K. Billimoria, Y. A. D. Fernandez, E. Andresen, I. Sorzabal-Bellido, G. Huelga-Suarez, D. Bartczak, C. Ortiz de Solórzano, U. Resch-Genger and H. G. Infante, *Metallomics*, 2022, **14**, mfac088.

27 N. Grijalba, A. Legrand, V. Holler and C. Bouvier-Capely, *Anal. Bioanal. Chem.*, 2020, **412**, 3113–3122.

28 A. Bazo, E. Bolea-Fernandez, A. Rua-Ibarz, M. Aramendía and M. Resano, *Anal. Chim. Acta*, 2024, **1331**, 343305.

29 L. Kronlachner, Z. Gajarska, P. Becker, D. Günther and A. Limbeck, *J. Anal. At. Spectrom.*, 2025, **40**, 467–477.

30 A. L.-S. Oliver, S. Baumgart, W. Bremser, S. Flemig, D. Wittke, A. Grützkau, A. Luch, A. Haase and N. Jakubowski, *J. Anal. At. Spectrom.*, 2018, **33**, 1256–1263.

31 A. Bazo, E. Bolea-Fernandez, A. Rua-Ibarz, M. Aramendía and M. Resano, *Anal. Chem.*, 2025, **97**, 13922–13929.